

CANDELS: STRONG LENSING GALAXIES IN HST/WFC3 IMAGING DATA OF UDS AND GOODS-S

ASANTHA COORAY^{1,†}, HAI FU¹, JAE CALANOG¹, J. L. WARDLOW¹, A. CHIU¹, S. KIM¹, J. SMIDT¹, V. ACQUAVIVA², H. C. FERGUSON³, S. M. FABER⁴, A. GALAMETZ⁵, N. A. GROGIN³, W. HARTLEY⁶, D. KOCEVSKI⁴, A. KOEKEMOER³, D. C. KOO⁴, R. A. LUCAS³, L. MOUSTAKAS⁷, J. A. NEWMAN⁸

Draft version October 9, 2018

ABSTRACT

We present results from a search for gravitationally lensed galaxies present in the *Hubble Space Telescope* (HST)/Wide Field Camera-3 (WFC3) images of the Cosmic Assembly Near-IR Deep Extragalactic Legacy Survey (CANDELS). We present one bona fide lens system in UDS and two compact lens candidates in the GOODS-S field. The lensing system in UDS involves two background galaxies, one at $z = 1.847$ lensed to an arc and a counterimage, and the second at a photometric redshift of $z = 2.32^{+0.10}_{-0.06}$ lensed to a double image. We reconstruct the lensed sources in the source plane and find in each of the two cases the sources can be separated to a pair of galaxies. The sources responsible for the arc are compact with effective radii of 0.3 to 0.4 kpc in WFC3 J_{125} -band and a total stellar mass and a star-formation rate of $2.1^{+2.4}_{-0.4} \times 10^7 M_{\odot}$ and $2.3^{+0.6}_{-1.7} M_{\odot} \text{ yr}^{-1}$, respectively. The abnormally high H_{160} -band flux of this source is likely due to [O III] emission lines with a rest-frame equivalent width about 700 Å for [O III] 5007 Å. The sources responsible for the double image have corresponding values of about 0.4 to 0.5 kpc, $1.4^{+1.9}_{-0.8} \times 10^9 M_{\odot}$ and $8.7^{+11.1}_{-7.0} M_{\odot} \text{ yr}^{-1}$. Once completed CANDELS is expected to contain about 15 lensing systems and will allow statistical studies on both lensing mass profiles and $z \sim 2$ lensed galaxies.

Subject headings: Gravitational lensing; strong

1. INTRODUCTION

Gravitational lensing is an invaluable tool in astrophysics. It has been exploited in the past to study properties of both the background lensed galaxies as well as the foreground lenses (see reviews by Bartelmann 2010; Treu et al. 2010). The variety of studies enabled by lensing has motivated searches for lensing events in various multi-wavelength astronomical datasets, from optical (e.g., SLACS: Bolton et al. 2006), sub-mm (e.g., *Herschel*: Negrello et al. 2010) to radio (CLASS: Browne et al. 2003). Given that most galaxy-scale lenses involve $\lesssim 1''$ image separations, most successful searches for gravitational lenses have involved the use of high resolution imaging. In this respect, *HST* surveys have been successful in uncovering lensed galaxies even in relatively small areas on the sky (Ratnatunga et al. 1995; Barkana et al. 1999; Fassnacht et al. 2004; Moustakas et al. 2007; More et al. 2011).

The CANDELS is now obtaining WFC3 and ACS imaging data of several well-known extragalactic fields at unprecedented depth and resolution (Grogin et al. 2011; Koekemoer et al. 2011). The early data include F125W,

F160W (WFC3), and F814W (ACS) imaging over an area of 249 arcmin² in GOODS-S and UDS fields. These initial imaging data are adequate for a first study of lensed galaxies. In comparison to the work we present here More et al. (2011) identified 10 candidate lensed galaxies using ACS imaging over 0.22 deg² of the ECDFS. Based on their success rate at identifying candidate lensing events, we expect about 3 to 4 lensed galaxies in current CANDELS data and about 15 when completed with imaging over 0.35 deg². Due to the ground-based and ACS data in CANDELS fields, we do expect some fraction of the lensed galaxies to be identified already.

The paper is organized as follows: In Section 2 we present a brief summary of the candidate lens selection. Section 3 describes surface brightness models, while in Section 4 we outline the lens models and discuss results on the three lens systems. For lensing models we assume the best-fit concordance cosmology consistent with WMAP-7 year data (Larson et al. 2011).

2. LENS CANDIDATE SELECTION

For the lens candidate search we make use of the CANDELS v0.5 drizzled mosaics at the pixel scale of 0.03 and 0.06''/pixel for WFC3 and ACS bands, respectively, and involving two epochs of UDS and five epochs of GOODS-S (wide)¹⁰ (Koekemoer et al. 2011). The UDS mosaic has 5 σ point source depths of 27.3, 26.3 and 25.9 (AB) magnitudes in F814W (I_{814} -band), F125W (J_{125} -band), and F160W (H_{160} -band), respectively. The corresponding depths for GOODS-S mosaics are 27.7, 26.6, and 26.5 (AB). As an initial search for lensed galaxies in the UDS and GOODS-S fields we created individual false-color postage stamps of $\sim 10^4$ potential lensing galaxies with $I \leq 26.5$ mag. Our selection of lensed candidates is simply based on morphological information only. For this, we inspected individual image cutouts searching for

[†] acooray@uci.edu

¹ Department of Physics & Astronomy, University of California, Irvine, CA 92697

² Department of Physics and Astronomy, Rutgers, The State University of New Jersey, Piscataway, NJ 08854

³ Space Telescope Science Institute, Baltimore, MD 21218

⁴ UCO/Lick Obs. and Department of Astronomy and Astrophysics, University of California, Santa Cruz, CA 95064 USA

⁵ INAF - Osservatorio di Roma, Via Frascati 33, I-00040, Monteporzio, Italy

⁶ School of Physics and Astronomy, University of Nottingham, University Park, Nottingham NG7 2RD, UK

⁷ Jet Propulsion Laboratory, California Institute of Technology, Pasadena, CA 91109

⁸ Department of Physics and Astronomy, University of Pittsburgh, Pittsburgh, PA

¹⁰ Mosaics are publicly available at <http://candels.ucolick.org/>

TABLE 1
PROPERTIES OF GOODS-S CANDIDATE LENSED SYSTEMS

Source	RA ^(a)	Dec ^(a)	$\mu^{(f)}$	R_{Einstein}	$\sigma_{\text{lens}}^{(b)}$	$R_e^{(g)}$	Sérsi c index n	$\epsilon^{(h)}$
GOODS-S01 $z_{\text{lens}} = 1.22^{(i)}$ (Dark matter) (lensed source)	53.019907°	-27.770704°		$0.53 \pm 0.06''$		$0.19 \pm 0.01''^{(c)}$	$0.31 \pm 0.01^{(c)}$	$0.748 \pm 0.005^{(c)}$
					$250 \pm 20^{(d)}$			$0.71^{+0.09}_{-0.12}^{(d)}$
			38^{+45}_{-6}			$0.08 \pm 0.01^{(e)}$	$1.2^{+1.0}_{-0.1}^{(e)}$	$0.35^{+0.55}_{-0.12}^{(e)}$
GOODS-S02 $z_{\text{lens}} = 1.02^{(i)}$ (Dark matter) (lensed source)	53.026810°	-27.791320°		$0.45 \pm 0.07''$		$0.324 \pm 0.003''^{(c)}$	$4.5 \pm 0.03^{(c)}$	$0.77 \pm 0.03^{(c)}$
					$216 \pm 9^{(d)}$			$0.50^{+0.27}_{-0.04}^{(d)}$
			10^{+35}_{-2}			$0.42^{+0.07}_{-0.03}''^{(e)}$	$1.8 \pm 0.3^{(e)}$	$0.89^{+0.09}_{-0.61}^{(e)}$

NOTE. — (a): Lensing galaxy centroids from GALFIT using F814W. (b): In units of km/sec. (c): For the I_{814} -band lens light profile from GALFIT using F814W. (d): for the lens dark matter profile from lens modeling. (e): for the lensed I_{814} -band background source light profile from lens reconstruction and GALFIT modeling. (f): Lensing magnification. (g): Effective radius from GALFIT modeling. (h): Axis ratio from GALFIT modeling. (i): Spectroscopic redshift from Vanzella et al. (2005).

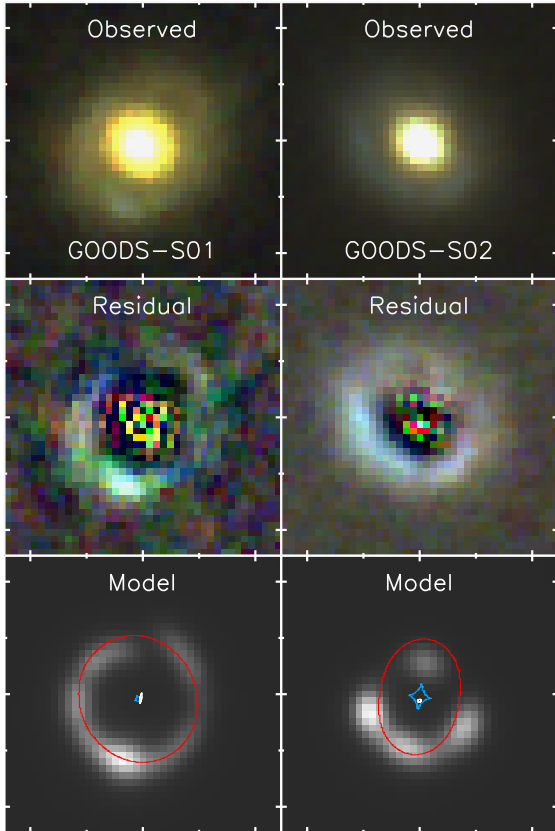


FIG. 1.— Lens candidates in GOODS-South (GOODS-S01 and GOODS-S02). The two columns are for the two candidates and from top to bottom we show *HST*/ACS I_{814} -band and WFC3 H - and J -band (RGB) pseudo-color images of the original and lens-subtracted residual images, and the best-fit lens model. The source position and shape is indicated by the white ellipse near the center of the right panels. The red and blue curves show the critical curve and the caustic. Each tick mark is $1''$.

both extended structure and color differences at the outskirts of galaxies that could be evidence for lensing. This process allowed us to make an initial selection of 20 candidate gravitationally lensed galaxies. Through an internal poll within the CANDELS team we ranked the list of 20 and selected three high priority targets for further studies reported in this paper.

The three lensing candidates are GOODS-S01 and GOODS-S02 (Table 1) and UDS-01 (Table 2). GOODS-S02 was identified by More et al. (2011) as a candidate lensing system and is included as their second highest priority lensing system from ACS images; The highest priority lensing

system from More et al. (2011) is not in our candidate list as CANDELS tiles do not overlap with it. GOODS-S01 was previously identified as a partial-ring galaxy in GEMS and GOODS Elmegreen & Elmegreen (2006).

UDS-01 was previously identified as a lensing galaxy by Geach et al. (2007) as part of a radio source followup. The lensed source was later identified in the CFHT Legacy Survey and was included in a snapshot *HST*/ACS lensing program for strong lenses in the CFHTLS (Tu et al. 2009). The CANDELS WFC3 imaging complements existing ACS data in V_{606} - (F606W) and I_{814} -band. Furthermore this field has both CFHTLS MegaCam imaging in the optical and UKIDSS WFCAM Ultra-Deep Survey (UDS) imaging in the near IR. CFHTLS images reach 5σ depths of 25.9, 26.5, 25.8, 26.0 and 24.6 magnitudes (AB), respectively, in u , g , r , i , and z respectively with typical seeing in the UDS-01 region of about 0.8 arcsec (FWHM). We also make use of J , H and K -band images from UKIDSS UDS data release 8 (Almaini et al. in prep.), which reach 24.9, 24.0 and 24.6 magnitudes (AB, 5σ with $2''$ aperture) respectively. The seeing FWHM in the region of UDS-01 range from $0.75''$ for the K -band data to $0.83''$ for H -band.

UDS-01 involves a foreground lens galaxy which is a member of a group/cluster potential at $z = 0.648$ and with a velocity dispersion of 770 km/sec Geach et al. (2007). The system involves two background lensed sources with one at a measured spectroscopic redshift of 1.847 and another with a previously estimated photometric redshift of $2.90^{+0.18}_{-0.24}$ in Tu et al. (2009) using CFHTLS and ACS V_{606} - and I_{814} -band data. We revise this estimate to be $2.32^{+0.10}_{-0.06}$ here with 12-band photometry involving CFHT (u , g , r , i , z), UKIDSS (J , H , K), ACS (V_{606} , I_{814}), and WFC3 (J_{125} , H_{160}).

3. SURFACE BRIGHTNESS MODELS

The two-dimensional surface brightness profile of each of the three foreground lensing galaxies were modeled using the GALFIT 3.0 routine (Peng et al. 2010) in order to perform the foreground lens-background source separation shown on Figs. 1 and 2. A $12 \times 12''$ region was cut out from each of the UDS and GOODS-S mosaics and was used as the input image for galaxy profile modeling.

For GALFIT modeling the foreground lensing galaxies were assumed to have a Sérsic profile of the form

$$\Sigma(R) = \Sigma_e \exp[-b_n((R/R_e)^{1/n} - 1)], \quad (1)$$

where R_e is the scale radius and n is the index. Since the only object of interest for GALFIT modeling was the lensing

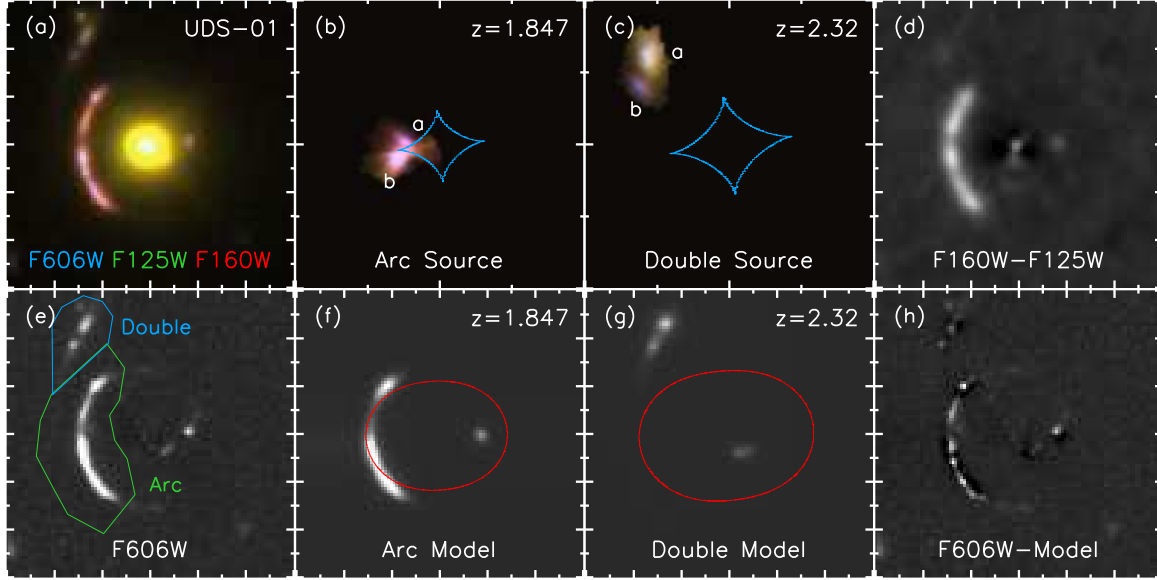


FIG. 2.— Double source plane system UDS-01. (a): *HST*/ACS I_{814} - and WFC3 J_{125} and H_{160} -band (RGB) pseudo-color image. (b) and (c): the lens reconstructed pseudo-color images of the sources responsible for the arc and double lensed images, respectively. The blue curve is the caustic at the respective source plane. We label the two components that are lensed to produce each of the arc and the double with ‘a’ and ‘b’; their properties are listed in Table 2. The corresponding lens models for V_{606} -band observations are shown in panels (f) and (g), where the red curve is now the critical line in the image plane. These best-fit models can be compared directly to lens-subtracted F606W image in panel (e). The difference between observed images and lensing models is shown in panel (h). (d): The difference between J_{125} scaled to H_{160} using the SED and the observed H_{160} . We believe this excess originates from strong [O III] 4959 an 5007 emission that falls in F160W filter for a source at $z = 1.847$. In panel (e) we show the irregular apertures used for photometry of the arc and north-west images of the double source to construct SEDs shown in Fig. 3. Each tick mark is $1''$; note that the reconstructed source images in (b) and (c) are zoomed-in relative to other panels. Through lensing magnification, we have achieved a spatial resolution of order $0.01''$ or 100 pc in the source plane.

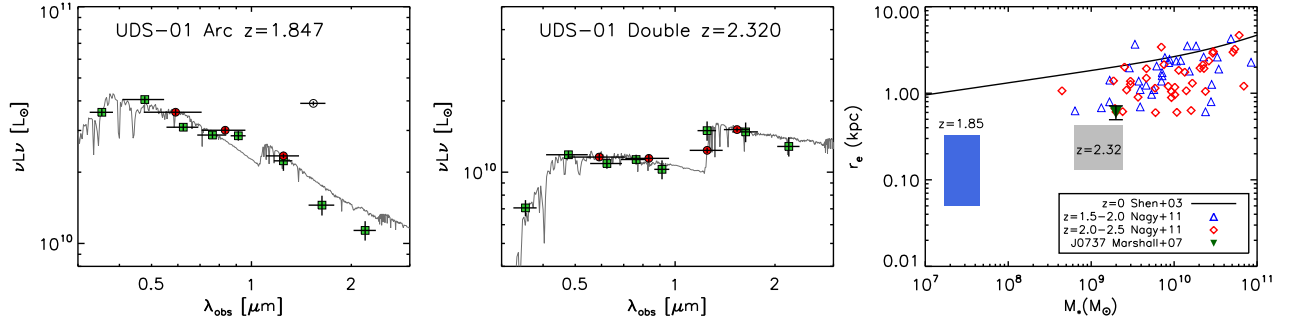


FIG. 3.— Spectral energy distribution (SED) of the arc (left) and north-west images of the double (middle). The luminosity scale is magnification corrected. The photometry points are from *HST* (circles) and CFHT and UKIDSS (squares). The curves show the best-fit SED using Bruzual & Charlot (2003) templates. Right: The size-stellar mass relation of $1.5 < z < 2.5$ galaxies. The two boxes mark the allowed 68% confidence range of the sources that produce the arc and the double source. The open triangles show the measurements at $1.5 < z < 2.5$ by Nagy et al. (2011) using WFC3 F160W. The filled triangle is a previous result on a lensing galaxy at $z = 0.58$ (Marshall et al. 2007). The solid line is the $z = 0$ relation from SDSS (Shen et al. 2003). We use WFC3 F125W here for the size measurement as F160W flux has [O III] emission lines.

galaxy for each image, all other sources including the lensed sources were masked for this purpose.

To improve the accuracy and decrease the level of degeneracy of the morphological parameters such as the integrated magnitude, Sérsic index, and effective radius, PSFs for WFC3 data generated internally by CANDELS (Koekemoer et al. 2011) were used as an input for convolution in the modeling. *HST*/WFC3 noise rms maps were also utilized instead of GALFIT’s internal sigma image generating algorithm to improve the uncertainties reported in the output parameters. The residual after accounting for the central lensing galaxy profile is taken to be the lensed flux of the background source. These residual images are used directly in lens modeling.

4. LENS MODELS AND RESULTS

We use the publicly available *Lenstool* software (Jullo et al. 2007) in combination with the IDL routine AMOEBA_SA to optimize the lens model and the shape of the lensed galaxy.

For the candidate lenses GOODS-S01 and GOODS-S02, we assume that each of the foreground lens galaxies is embedded in a dark matter halo that can be described as an elliptical singular isothermal sphere (SIS). The halos are fixed to the centroids of the galaxies as determined from GALFIT. For the lensed galaxies, we assume exponential disk profiles with $\Sigma(r) = \Sigma_0 \exp(-r/r_s)$. There are a total of nine free parameters — the position, the intrinsic magnitude, the scale length, the ellipticity, and the position angle (PA) of the source (x , y , m_s , r_s , $\epsilon_s = 1 - b/a$, and ϕ_s), and the ellipticity, the PA, and the velocity dispersion of the dark matter halo (ϵ_d , ϕ_d , and σ_{SIS}).

UDS-01 is a more complicated case. The central lensing

TABLE 2
PROPERTIES OF THE UDS-01 LENSING SYSTEM

Quantity	Value	Ref
Lens Galaxy		
RA	34.404790°	ACS I_{814} -band
Dec	-5.224868°	ACS I_{814} -band
Redshift	0.6459 ± 0.0003	Tu et al. 2009
σ_{SIE}	280.1 ± 0.3 km s ⁻¹	lens model
$R_{Einstein}$	1.183 ± 0.005''	lens model
ϵ_d	0.879 ± 0.004	lens model
PA_d	73.5 ± 10°	lens model
R_e	1.170 ± 0.004''	GALFIT
	8.14 ± 0.03 kpc	
ϵ_s	0.918 ± 0.002	GALFIT
n (Sérsic)	8.0 ^(I)	GALFIT
Lens Cluster		
RA	34.389725°	Geach et al. 2007
Dec	-5.220814°	Geach et al. 2007
Redshift	0.648 ± 0.001	Geach et al. 2007
σ_{SIS}	774 ± 170 km s ⁻¹	Geach et al. 2007
Tangential Arc		
Redshift	1.8470 ± 0.0003	Tu et al. 2009
ACS/F606W	22.28 ± 0.03	Photometry
ACS/F814W	22.12 ± 0.03	
WFC3/F125W	21.89 ± 0.02	
WFC3/F160W	21.11 ± 0.02	
RA ^(II)	34.402409°	lens model
Dec ^(II)	-5.224189°	lens model
μ (a)	50 ⁺⁸ ₋₄	lens model
n (a)	1.05 ± 0.25	GALFIT/lens reconstruction
R_e (a)	0.008 ± 0.003''	GALFIT/lens reconstruction
	0.06 ± 0.02 kpc	(in F125W)
ϵ (a)	0.79 ^{+0.19} _{-0.38}	GALFIT/lens reconstruction
μ (b)	40 ⁺² ₋₃	lens model
n (b)	1.26 ± 0.13	GALFIT/lens reconstruction
R_e (b)	0.036 ± 0.004''	GALFIT/lens reconstruction
	0.31 ± 0.02 kpc	(in F125W)
ϵ (b)	0.93 ^{+0.05} _{-0.32}	GALFIT/lens reconstruction
M_*	2.1 ^{+2.4} _{-0.4} × 10 ⁹ M _⊙ ^(III)	SED/lens magnification
SFR	2.3 ^{+0.6} _{-1.7} M _⊙ yr ⁻¹ ^(III)	SED/lens magnification
E(B-V)	0.25 ^{+0.02} _{-0.08}	SED/lens magnification
Double System		
Redshift	2.32 ^{+0.10} _{-0.06}	photo-z
ACS/F606W	24.06 ± 0.04	Photometry
ACS/F814W	23.72 ± 0.04	
WFC3/F125W	23.14 ± 0.03	
WFC3/F160W	22.69 ± 0.02	
RA ^(II)	34.402245°	lens model
Dec ^(II)	-5.223925°	lens model
μ (a)	2.9 ± 0.2	lens model
n (a)	1.35 ± 0.25	GALFIT/lens reconstruction
R_e (a)	0.05 ± 0.01''	GALFIT/lens reconstruction
	0.5 ± 0.1 kpc	(in F125W)
ϵ (a)	0.73 ^{+0.23} _{-0.25}	GALFIT/lens reconstruction
μ (b)	3.4 ± 0.1	lens model
n (b)	1.50 ± 0.25	GALFIT/lens reconstruction
R_e (b)	0.02 ± 0.01''	GALFIT/lens reconstruction
	0.2 ± 0.08 kpc	(in F125W)
ϵ (b)	0.79 ^{+0.19} _{-0.38}	GALFIT/lens reconstruction
M_*	1.4 ^{+1.0} _{-0.4} × 10 ⁹ M _⊙ ^(III)	SED/lens magnification
SFR	8.7 ^{+11.1} _{-7.0} M _⊙ yr ⁻¹ ^(III)	SED/lens magnification
E(B-V)	0.29 ^{+0.08} _{-0.12}	SED/lens magnification

NOTE. — (I): GALFIT models converge when $n > 4$. (II): Position of the best-fit brightest source component from lens modeling using F125W (WFC3 J_{125} -band) image. (III): Corrected for lensing magnification.

galaxy at $z = 0.6459$ belongs to an X-ray detected galaxy group at $z = 0.648$. Hence, besides the elliptical SIS halo centered on the lensing galaxy, we also include a circular SIS halo at the center of the galaxy group 56'' NW of UDS-01 with its velocity dispersion fixed to that of the member galaxies (774 km s⁻¹ at $z = 0.648$ Geach et al. 2007). In addition, there are

two pairs of background galaxies that are strongly lensed by the joint gravitational potential of the central galaxy and the group: one at $z = 1.847$ corresponding to the tangential arc, the other at a photometric redshift of $z \sim 2.32$ corresponding to the double system further out (see Fig. 2). Because the tangential system provides better constraints to the dark matter distribution, we use the tangential system to find the parameters of the SIS halo associated with the central lensing galaxy, then we use this solution to constrain the positions and shapes of the double system. Again we assume exponential profiles for the background galaxies.

Our fitting procedure is as follows. For an initial set of parameters describing the source and the deflector, we use `Lenstool` to generate a deflected image of the source. We then convolve it with the WFC3 PSFs at each band and subtract it from the observed lens-subtracted image to compute the χ^2 value. This process is iterated with `AMOEBAS` to find the parameters that minimize the χ^2 value. `AMOEBAS` is based on the IDL multidimensional minimization routine `AMOEBAS` with simulated annealing added (E. Rosolowsky, private communication). We adopt an initial "temperature" of 100 and decrease it by 40% in each subsequent calls of `AMOEBAS`.

4.1. GOODS-S01 and GOODS-S02

Fig. 1 shows the best-fit lensing models for the Einstein ring candidate GOODS-S01 and the cusp lens GOODS-S02 and Table 1 summarizes lens model properties. For lens modeling, we assume that the background galaxies in both systems are at $z = 2$. We attempted to extract the photometric redshift of the background galaxies by SED fitting to CANDELS and archival residual fluxes. Both systems, however, are compact with each having an Einstein radius of $\sim 0.5''$ and an accurate separation of the lens profile from the background source flux was challenging. The reduced- χ^2 value for the best-fit lens model is 1.1 and 1.5 for GOODS-S01 and -S02, respectively.

The dark matter profile of GOODS-S02 lens has an ellipticity of $0.50^{+0.27}_{-0.04}$, while the Einstein radius is $0.45 \pm 0.07''$. These are consistent with values of 0.48 and $0.4''$ reported in More et al. (2011), respectively. The lens galaxies have effective radii of 0.64 ± 0.08 kpc (GOODS-S01) and 0.38 ± 0.04 kpc (GOODS-S02). Using the best-fit velocity dispersion and axis ratios, we estimate enclosed masses within critical (Einstein) radii of $(4.8 \pm 1.8) \times 10^{11}$ M_⊙ and $(3.8 \pm 1.7) \times 10^{11}$ M_⊙ for GOODS-S01 and S02, respectively. The corresponding I_{814} -band luminosities for apertures matched to the critical radii of the two galaxies are $(7.1 \pm 0.3) \times 10^{10}$ L_⊙ and $(1.1 \pm 0.3) \times 10^{11}$ L_⊙. We find total mass-to-light ratios of 6.7 ± 1.1 and 3.5 ± 1.6 out to critical radii of GOODS-S01 and S02, respectively. Note that there is an additional systematic error of ± 1.5 to 2.0 in the M/L ratio associated with the unknown background source redshifts for the two lens systems.

4.2. UDS-01

Fig. 2 shows the best-fit lens model and the lensed galaxy image reconstruction directly in the source plane. Table 2 summarizes lens modeling, profile fitting, and SED modeling results. To measure source properties we make use of WFC3/F125W image. The arc and counterimage, taking the form of a cusp lens, involve an extend source with at least two peaks of emission. The source responsible for double image is also made up of two separate galaxies in the source plane.

In Table 2 we separate the properties of each of these galaxy pairs with labels (a) and (b), while the two components are identified in Fig. 2(b) and (c) panels.

In Fig. 3 we show the SEDs of the sources responsible for the lensed arc and the north-west double source, with the luminosity scale corrected for the magnification. In making these SED plots, instead of using GALFIT to remove the lens galaxy, we take advantage of the asymmetry of the lensed system and create residual images by subtracting a mirrored image from the original image. This removes the need for accurate galaxy profiles for the lens. Irregular-sized apertures are made to enclose most of the flux from the arc and the NW-double in the CFHT and UKIDSS images as highlighted in Fig. 2(e). The WFC3/F160W photometry of the arc is abnormally high. This is probably due to the redshifted [O III] 4959 and 5007 lines, as both fall within the WFC F160W band for a source at $z = 1.847$. This hypothesis is supported by the fact that the bandpass in WFC3 begins at $1.4 \mu\text{m}$, while UKIRT WFCAM H -band filter used in UKIDSS has effectively a zero throughput at $\lambda < 1.45 \mu\text{m}$ and misses the [O III] emission lines.

Stellar population synthesis models are built for exponentially declining star formation histories with $\text{SFR}(t) \propto \exp(-t/\tau)$ with various τ and ages (Bruzual & Charlot 2003), with the restriction that template ages are less than the age of the universe at the corresponding redshift. For each template we fit for stellar mass and intrinsic extinction to match the observed SEDs, assuming the extinction law of Calzetti et al. (1994) and parameterized by $E(B-V)$. The templates that gives the minimum χ^2 values are chosen as the best fit. Since the SED templates do not include emission lines, we did not include the F160W data point for $z = 1.847$ source in the modeling. The quoted best-fit stellar masses and SFRs are corrected for magnification using amplification factors calculated for the photometry apertures using the best-fit lensing model (Table 2).

We measure the difference of SED predicted flux scaled from F125W filter to F160W and the observed F160W flux as a measurement of the [O III] intensity. Fig. 2(d) shows that this difference is not localized to a specific region on the arc suggesting that the [O III] emission is spatially distributed broadly across the two components responsible for the arc. Assuming [O III] 4959 to 5007 ratio is 0.33, we estimate $F_\lambda(5007) \sim 8.9 \times 10^{-19} \text{ ergs s}^{-1} \text{ cm}^{-2} \text{ \AA}^{-1}$ and a rest-frame equivalent width for the [O III] emission of $\sim 700 \text{ \AA}$. The suggestion that the arc has high [O III] emission is consistent with the discovery of star-bursting dwarf galaxies in

CANDELS with strong [O III] emission lines falling in the WFC3 J_{125} -band (van der Wel et al. 2011). Our source is at a slightly higher redshift with [O III] in the WFC3 H_{160} -band. The van der Wel et al. (2011) sources have rest-frame equivalent widths as high as 1000 \AA and [O III] fluxes a factor of 3 to 4 higher than that of the arc after correcting for magnification. The stellar mass and the SFR we find the arc source with SED fits are consistent with the suggestion that the two sources are dwarf galaxies with a star-burst phase with M_*/SFR of around 9 to 10 Myr.

Based on GALFIT modeling of the reconstructed source profile, the sources responsible for the arc are compact with effective radii around 0.05 to 0.5 kpc, while the two sources responsible for the double images have effective radii of 0.2 to 0.6 kpc. In Fig. 3 right panel we summarize these sources in the stellar mass-size and compare to other samples of galaxies. As summarized there the arc sources are not only dwarf galaxies, or smaller than typical “dwarf” galaxies with a few times $10^7 M_\odot$ stellar mass, the galaxies are bursting with stars and have high [O III] emission. The lensing system is radio bright (Geach et al. 2007) and thus a high resolution map of the radio emission will be useful to have to narrow down the source of [O III] emission, especially if either or both of the two compact, star-bursting galaxies magnified to the arc host an AGN.

To summarize this *Letter*, we have presented results from a search for lensed galaxies in early CANDELS imaging data involving two candidates in GOODS-South and a bona fide lensing system in the UDS field. We reconstruct the lensed sources in the UDS system and through GALFIT and SED model fits to the total aperture fluxes establish their properties including effective radius, stellar mass, star-formation rate, among others. The pair of galaxies lensed to the arc and a counterimage show bright [O III] line emission in the WFC H_{160} -band. The sources are compact and are undergoing a star-bursting phase. They are some of the smallest galaxies with lowest stellar masses at $z > 1.5$ and falls below in size and stellar mass when compared to even dwarf galaxies at these redshifts.

Financial support for this work was provided by NASA through grant HST-GO-12060 from the Space Telescope Science Institute, which is operated by Associated Universities for Research in Astronomy, Inc., under NASA contract NAS 5-26555. Partly based on observations obtained with CFHT/MegaCam. The UKIDSS project is defined in Lawrence et al. (2007).

REFERENCES

- Barkana, R., Blandford, R., & Hogg, D. W. 1999, *ApJ*, 513, L91
 Bartelmann, M. 2010, *Classical and Quantum Gravity*, 27, 233001
 Bolton, A. S., Burles, S., Koopmans, L. V. E., Treu, T., & Moustakas, L. A. 2006, *ApJ*, 638, 703
 Browne, I. W. A., et al. 2003, *MNRAS*, 341, 13
 Bruzual, G., & Charlot, S. 2003, *MNRAS*, 344, 1000
 Calzetti, D., Kinney, A. L., & Storchi-Bergmann, T. 1994, *ApJ*, 429, 582
 Elmegreen, D. M. & Elmegreen, B. G. 2006, *ApJ*, 651, 676
 Fassnacht, C. D., Moustakas, L. A., Casertano, S., Ferguson, H. C., Lucas, R. A., & Park, Y. 2004, *ApJ*, 600, L155
 Geach, J. E., Simpson, C., Rawlings, S., Read, A. M., & Watson, M. 2007, *Monthly Notices of the Royal Astronomical Society*, 381, 1369
 Grogin, N. A., et al. 2011, *ArXiv e-prints*
 Jullo, E., Kneib, J. P., Limousin, M., Eliaodottir, A., Marshall, P. J., & Verdugo, T. 2007, *New Journal of Physics*, 9
 Koekemoer, A. M., et al. 2011, *ArXiv e-prints*
 Larson, D., et al. 2011, *ApJS*, 192, 16
 Lawrence, A., et al. 2007, *MNRAS*, 379, 1599
 Marshall, P. J., et al. 2007, *ApJ*, 671, 1196
 More, A., Jahnke, K., More, S., Gallazzi, A., Bell, E. F., Barden, M., & Häusler, B. 2011, *ApJ*, 734, 69
 Moustakas, L. A., et al. 2007, *ApJ*, 660, L31
 Nagy, S. R., Law, D. R., Shapley, A. E., & Steidel, C. C. 2011, *ApJ*, 735, L19
 Negrello, M., et al. 2010, *Science*, 330, 800
 Peng, C. Y., Ho, L. C., Impey, C. D., & Rix, H.-W. 2010, *AJ*, 139, 2097
 Ratnatunga, K. U., Ostrander, E. J., Griffiths, R. E., & Im, M. 1995, *ApJ*, 453, L5+
 Shen, S., et al. 2003, *MNRAS*, 343, 978
 Treu, T. 2010, *ARA&A*, 48, 87
 Tu, H., et al. 2009, *A&A*, 501, 475
 van der Wel, A., et al. 2011, *ArXiv e-prints*
 Vanzella, E., et al. 2005, *A&A*, 434, 53